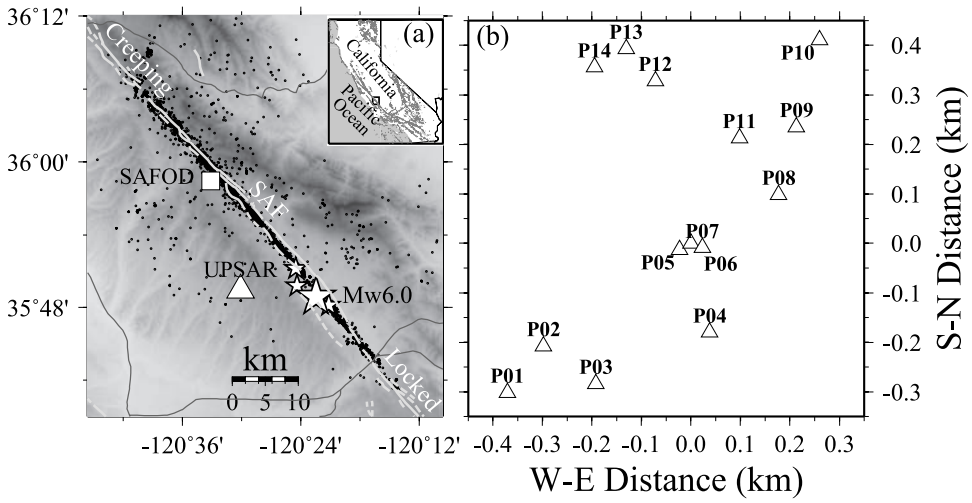

Figure 1. (a) Map view of San Andreas Fault near Parkfield, CA. The 2004 M6 Parkfield earthquake and large early aftershocks are indicated by stars and other aftershocks are shown as dots. The thick gray and light lines denote surface traces of SAF and nearby roads, respectively. The background is shaded topography with white being low and dark being high. The locations of the USGS Parkfield Dense Seismograph Array (UPSAR) and the SAFOD are denoted by the inverted triangle and square, respectively. The inset shows the study area on a map of California. (b) Small scale view of UPSAR stations. The distances are relative to station P06.

[*Fletcher et al.*, 1992]. These recordings are ideal for searching for dynamically triggered high-frequency bursts during the strong shaking associated with the Parkfield earthquake sequence.

[7] We searched for bursts by applying a 4th order Butterworth high-pass filter with a cutoff frequency of 20 Hz to all the strong motion recordings from the 12 active stations during the first 900 seconds of the Parkfield earthquake sequence (Figure 2). We chose 20 Hz as a lower cutoff because seismic energy above this frequency attenuates very quickly and is less likely to be contaminated by radiation from the mainshock source region, and because this is the frequency range in which high-frequency bursts were observed in Taiwan [*Chen et al.*, 2006; *Fischer et al.*, 2008]. We observed high-frequency bursts on the filtered records from all three components of all 12 stations during the strong shaking from the Parkfield mainshock (Figures 2–3 and S1[1]–S3).The amplitudes and durations of these bursts are similar to those observed in Taiwan [*Chen et al.*, 2006; *Fischer et al.*, 2008]. Bursts were also observed during strong shaking associated with three largest immediate aftershocks ($Mw \geq 4$) at Parkfield, but not during the relatively quiet periods between these events.

[8] Although *Peng et al.* [2006] used a similar high-pass filtering technique to identify many early aftershocks in the source region that were not in the standard earthquake catalogs, it is evident from Figure 2 that the bursts observed here are different in that they are not clearly correlated at different stations in the array. Even the largest amplitude burst observed during the Parkfield mainshock cannot be clearly identified at any nearby station, although there are many small amplitude events at about the same time that might be correlated (see, for example, the large burst at station P10 in Figure 2 at ~8 s). This first-order observation suggests that the high-frequency bursts are most likely due to a phenomenon located very near each station.

3. Burst Identification Algorithm

[9] Our automated algorithm for identifying bursts generally follows that by *Fischer et al.* [2008] and is briefly described here. The accelerograms were first high-pass filtered at 20 Hz using a 4th order Butterworth filter. Bursts were identified using an algorithm that imposed an amplitude threshold based on the SNR. Local minima and maxima were found by differentiation and local extrema that exceeded the amplitude threshold were saved. If any two saved picks occurred within 0.2 seconds of each other, they were considered as a single event. We also required that a burst appear on all three components.

[10] This algorithm picked bursts that were obvious by visual inspection, but it also picked events that were not obvious or appeared as a relatively continuous "tremor-like" signal [e.g., *Obara*, 2002]. Most of these questionable picks were eliminated by increasing the SNR threshold and paying the penalty of reducing the total number of identified bursts. We found that a SNR of 50 gave the best agreement with visual inspection.

[11] We used this algorithm to search for bursts on the records from all 12 operating UPSAR stations during a 900 second interval that include the Parkfield mainshock and its early aftershocks. We found 648 high-frequency bursts using the SNR = 10, 136 bursts using SNR = 50, and 44 bursts using SNR = 100.

4. Triggering Threshold

[12] If the high-frequency bursts originate in the shallow crust very near the stations and are dynamically triggered by strong ground motions [*Fischer et al.*, 2008], then the triggering threshold can be estimated by calculating the

[1]Auxiliary materials are available in the HTML. doi:10.1029/2008GL033905.

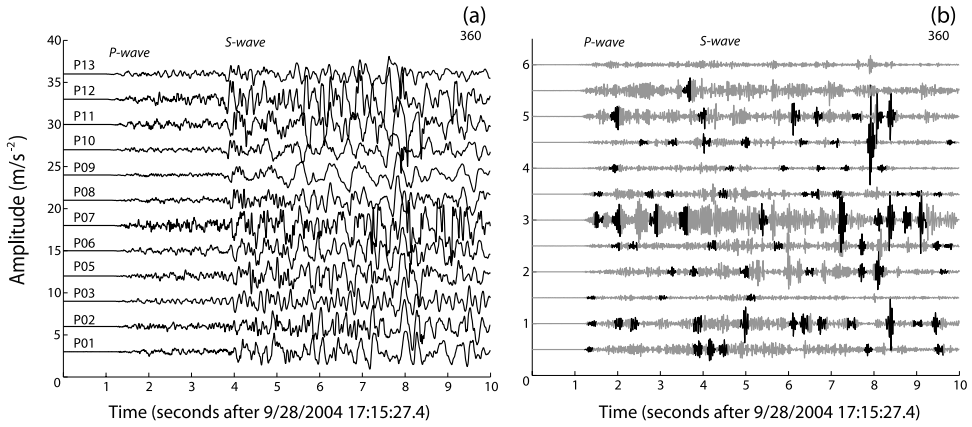

Figure 2. (a) Raw and (b) 20-Hz high-pass-filtered north-component acceleration seismograms recorded by the UPSAR during the first 10 s of the 2004 Parkfield earthquake. The station name is marked on the left. The high-frequency bursts picked by our automated algorithm with a signal-to-noise ratio of 50 are indicated in black in Figure 2b. Records are lined up with the origin time of the Parkfield mainshock as indicated. P- and S-wave arrivals are indicted on the figure for reference.

maximum dynamic stress in the seismic waves just prior to the arrival of each burst. For plane waves, the peak dynamic stress σ_d is equal to ν G/β [*Hill and Prejean*, 2007], where G is the shear modulus, ν is the peak particle velocity, and β is the shear-wave velocity. Values of ν were obtained by integrating the strong motion acceleration records. The triggering stress of a burst was defined as the maximum value of σ_d, on all three components, within a 1 second window prior to its arrival. Similar instantaneous triggering was observed during the passage of surface waves generated by the 2002 Denali earthquake [*Prejean et al.*, 2004; *Gomberg et al.*, 2008], and 2004 Sumatra earthquake [e.g., *Miyazawa and Brodsky*, 2008]. Repeating the calculations with longer time windows did not produce a significant change in the threshold.

[13] Figure 4 shows the distributions of triggering stresses for different SNR. Taking G = 0.3 GPa and β = 326 m/s [*Fletcher et al.*, 2006] for the shallow crust, gives a stress amplitude threshold of 0.02 MPa for SNR = 50. We define the threshold as the stress level above which 95% of bursts are triggered. These stresses are consistent with the range of 0.03 to 0.05 MPa obtained from the high-frequency triggering analysis of bursts observed during strong motion from the Chi-Chi earthquake [*Fischer et al.*, 2008].

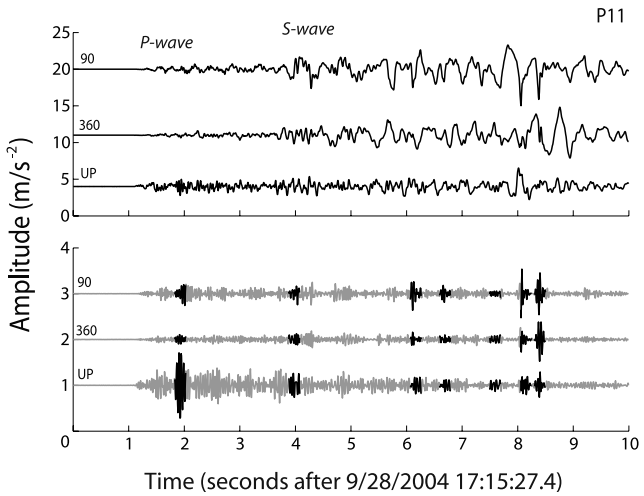

Figure 3. (top) Raw and (bottom) 20-Hz high-pass-filtered three-component seismograms recorded by station P11 during the first 10 s of the Parkfield mainshock. The high-frequency bursts picked by our automated algorithm with a signal-to-noise ratio of 50 are indicated in black.

5. Location and Size of the Bursts

[14] In the Taiwan study [*Fischer et al.*, 2008], observed a lack of correlation across a sub-array with average station spacing of 3 km. The failure to identify a burst on more than one station implied they were within 750 meters of the

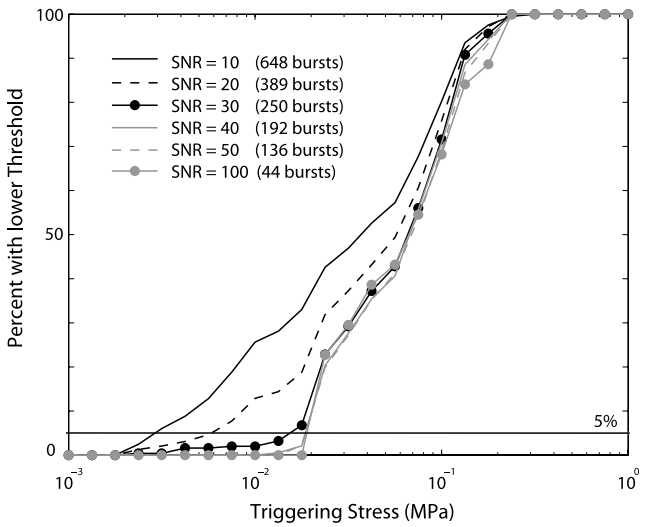

Figure 4. Triggering threshold for a range of signal-to-noise ratios (SNR). The horizontal line indicates the 95% Threshold. The intersection of this line with the curves indicates the triggering stress. For our preferred SNR = 50, the threshold is 0.02 MPa. For SNR > 30, triggering thresholds cluster about our preferred value of 0.02 MPa at SNR = 50.

station and that the magnitude had to be below $Mw = 0$. The nearest neighbors in the UPSAR array are 40 meters apart. Lack of correlated bursts at UPSAR implies that they are within 20 meters of a station and the magnitude of the largest amplitude burst has $Mw = -1$ and corresponding seismic potency $Po = 1.2 \times 10^{-5}$ km^{2}cm, where this magnitude was determined from the spectral amplitude in the low frequency limit. Because the spectrum is contaminated by energy from the Parkfield mainshock at low frequency, we assumed that the spectral amplitude at 10 Hz gives an adequate approximation to the magnitude. It is of interest to note that for vertically propagating SH-waves, peak dynamic stresses are found at the 1/4 wavelength depth [*Sleep and Ma*, 2008]. The dominant frequency from the average spectrum of all the records is about 2 Hz.. The corresponding wavelength with the near-surface S-wave velocity $\beta = 326$ m/s is about 140 m, and the 1/4 wavelength is about 35 m. This value is close to the distance where we think the bursts are produced.

6. Discussion

[15] In this study we observed many high-frequency bursts during strong motion from the 2004 Parkfield earthquake and its immediate largest aftershocks recorded by the UPSAR array. After investigating and ruling out several possible artifacts associated with instruments (see Text S1), we hypothesize that these signals are generated by sources within 20 m of the receivers that were dynamically triggered by the strong ground motion. This hypothesis is supported by three lines of evidence. First, the high-frequency bursts were only observed during the strong shakings (Figure 4). Second, although an individual burst was recorded on all three components of a given station, it could not be identified at other nearby stations (Figures 2 and 3). This lack of correlation is most likely due to the relatively small amplitudes and high-frequencies of the bursts, and to the extremely high attenuation in the highly fractured and weathered uppermost crust. Third, the threshold stress required for triggering found here (0.02 MPa) is consistent with a previous estimate for bursts triggered by 1999 Chi-Chi earthquake in Taiwan [*Fischer et al.*, 2008].

[16] Recent studies using repeating earthquakes have found reduced seismic velocities in the top few hundred meters of the crust associated with strong motions from nearby large earthquakes [e.g., *Rubinstein and Beroza*, 2005; *Peng and Ben-Zion*, 2006]. The reductions are most likely caused by the opening of pre-existing cracks during dynamic shaking, and are typically followed by logarithmic recovery. We speculate that this cracking process is accompanied by frictional loss from discrete events that reradiate energy to higher frequencies, some of which are recorded as high-frequency bursts by nearby stations. Large, but very rare bursts have been identified in the Parkfield region [*Sleep and Ma*, 2008] and have implications for theoretical limits of ground motion. In contrast, the numerous small high-frequency events observed in our study may be ubiquitous and play an important role in the attenuation of strong motion in the shallow crust.

[17] **Acknowledgments.** We thank Joe Fletcher, Paul Spudich, and Larry Baker for making the waveforms of the UPSAR available. We thank Dominic Assimaki for pointing out the work of *Bonilla et al.* [2005]. This work has benefitted from helpful reviews by John Vidale, Paul Spudich, and Norm Sleep. This research was supported by the Southern California Earthquake Center. SCEC is funded by NSF Cooperative Agreement EAR-0106924 and USGS Cooperative Agreement 02HQAG0008. The SCEC contribution number for this paper is 1201.

References

Aster, R. C., and P. M. Shearer (1991), High-frequency borehole seismograms recorded in the San Jacinto fault zone, southern California. Part 2. Attenuation and site effects, *Bull. Seismol. Soc. Am.*, *81*, 1081–1100.

Blakeslee, S., and P. Malin (1991), High-frequency site effects at two Parkfield downhole and surface stations, *Bull. Seismol. Soc. Am.*, *81*, 332–345.

Bonilla, L. F., R. J. Archeleta, and D. Lavellee (2005), Hysteretic and dilatant behavior of cohesionless soils and their effects on nonlinear site response: Field data observations and modeling, *Bull. Seismol. Soc. Am.*, *95*, 2373–2395.

Cranswick, E. (1988), The information content of high-frequency seismograms and the near-surface geologic structure of "hard rock" recording sites, *Pure Appl. Geophys.*, *128*, 333–363.

Chen, Y., C. G. Sammis, and T.-L. Teng (2006), A high frequency view of the 1999 Chi-Chi, Taiwan, source rupture and fault mechanics, *Bull. Seismol. Soc. Am.*, *96*, 807–820.

Ebel, J. E. (1989), The effect of crustal scattering on observed high-frequency earthquake seismograms, *Geophys. J. Int.*, *98*, 329–341.

Fischer, A. D., C. G. Sammis, Y. Chen, and T. L. Teng (2008), Dynamic triggering by strong motion *P*- and *S*-waves: Evidence from the 1999 Chi-Chi, Taiwan earthquake, *Bull. Seismol. Soc. Am.*, *98*, 580–592.

Fletcher, J. P., P. Spudich, P. Goldstein, J. Sims, and M. Hellweg (1992), The USGS Parkfield, California dense seismograph array–UPSAR, *Bull. Seismol. Soc. Am.*, *82*, 1041–1070.

Fletcher, J. P., P. Spudich, and L. M. Baker (2006), Rupture propagation of the 2004 Parkfield, California, earthquake from observations at the UPSAR, *Bull. Seismol. Soc. Am.*, *96*, S129–S142, doi:10.1785/01200050812.

Frankel, A. D., D. L. Carver, and R. A. Williams (2002), Nonlinear and linear site response and basin effects in Seattle for the *M*6.8 Nisqually, Washington, earthquake, *Bull. Seismol. Soc. Am.*, *92*, 2090–2109.

Gomberg, J., J. L. Rubensteing, Z. Peng, K. C. Creager, J. E. Vidale, and P. Bodin (2008), Widespread triggering of nonvolcanic tremor in California, *Science*, *319*, 173, doi:10.1126/science.1149164.

Hanks, T. C. (1982), f_{max}, *Bull. Seismol. Soc. Am.*, *72*, 1867–1880.

Hill, D. P., and S.G. Prejean (2007), Dynamic triggering, in *Treatise on Geophysics,* vol. 4, *Earthquake Seismology,* edited by H. Kanamori, pp. 257–292, *Elsevier*, Amsterdam.

Hill, D., et al. (1993), Seismicity remotely triggered by the magnitude 7.3 Landers, California, earthquake, *Science*, *260*, 1617–1623.

Holzer, T. L., T. L. Youd, and T. C. Hanks (1989), Dynamics of liquefaction during 1987 Superstition Hills, California, earthquake, *Science*, *244*, 56–59.

Langbein, J., et al. (2005), Preliminary report on the 28 September 2004, *M*6.0 Parkfield, California earthquake, *Seismol. Res. Lett.*, *76*, 10–26.

Miyazawa, M., and E. E. Brodsky (2008), Deep low-frequency tremor that correlates with passing surface waves, *J. Geophys. Res.*, *113*, B01307, doi:10.1029/2006JB004890.

Obara, K. (2002), Nonvolcanic deep tremor associated with subduction in southwest Japan, *Science*, *296*, 1681–1699.

Peng, Z., and Y. Ben-Zion (2006), Temporal changes of shallow seismic velocity around the Karadere-Duzce branch of the north Anatolian fault and strong ground motion, *Pure Appl. Geophys.*, *163*, 567–599.

Peng, Z., J. E. Vidale, and H. Houston (2006), Anomalous early aftershock decay rates of the 2004 *M*6 Parkfield earthquake, *Geophys. Res. Lett.*, *33*, L17307, doi:10.1029/2006GL026744.

Prejean, S. G., D. P. Hill, E. E. Brodsky, S. E. Hough, M. J. S. Johnston, S. D. Malone, D. H. Oppenheimer, A. M. Pitt, and K. B. Richards-Dinger (2004), Remotely triggered seismicity on the United States west coast following the *Mw* 7.9 Denali Fault earthquake: The 2002 Denali Fault earthquake sequence, *Bull. Seismol. Soc. Am.*, *94*, 348–359.

Rubinstein, J. L., and G. C. Beroza (2005), Depth constraints on nonlinear strong ground motion from the 2004 Parkfield earthquake, *Geophys. Res. Lett.*, *32*, L14313, doi:10.1029/2005GL023189.

Shearer, P. M., and J. A. Orcutt (1987), Surface and near-surface effects on seismic waves–theory and borehole seismometer results, *Bull. Seismol. Soc. Am.*, *77*, 1168–1196.

Sleep, N. H., and S. Ma (2008), Production of brief extreme ground acceleration pulses by nonlinear mechanisms in the shallow subsurface, *Geochem. Geophys. Geosyst.*, *9*, Q03008, doi:10.1029/2007GC001863.

Vernon, F. L., J. Fletcher, L. Carroll, A. Chave, and E. Sembrera (1981), Coherence of seismic body waves from local events as measured by a small-aperture array, *J. Geophys. Res.*, *96*, 11,981–11,996.

Vernon, F. L., G. L. Pavlis, T. J. Owens, D. E. McNamara, and P. N. Anderson (1998), Near-surface scattering effects observed with a high-frequency phased array at Pinyon Flats, California, *Bull. Seismol. Soc. Am.*, *88*, 1548–1560.

Wilson, D. C., and G. L. Pavlis (2000), Near-surface site effects in crystalline bedrock: A comprehensive analysis of spectral amplitudes determined from a dense, three-component seismic array, *Earth Interact.*, *4*. (Available at http://EarthInteractions.org)

A. D. Fischer and C. G. Sammis, Department of Earth Sciences, University of Southern California, Los Angeles, CA 90089–0740, USA. (adfische@usc.edu)

Z. Peng, School of Earth and Atmospheric Sciences, Georgia Institute of Technology, Atlanta, GA 30332, USA.